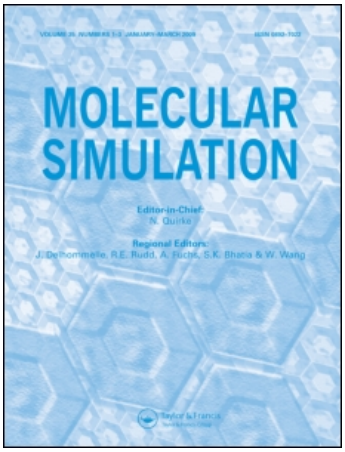

Molecular Simulation
Publication details, including instructions for authors and subscription information:
http://www.informaworld.com/smpp/title~content=t713644482

Molecular-level Calculation Scheme for Pressure in Inhomogeneous Systems of Flat and Spherical Layers

Tamio Ikeshoji[a]; BjØrn Hafskjold[ab]; Hilde Furuholt[b]
[a] Research Institute for Computational Sciences, National Institute of Advanced Industrial Science and Technology, Tsukuba, Japan [b] Department of Chemistry, Norwegian University of Science and Technology, Trondheim, Norway

Online publication date: 26 October 2010

To cite this Article Ikeshoji, Tamio , Hafskjold, BjØrn and Furuholt, Hilde(2003) 'Molecular-level Calculation Scheme for Pressure in Inhomogeneous Systems of Flat and Spherical Layers', Molecular Simulation, 29: 2, 101 — 109
To link to this Article: DOI: 10.1080/10286202100002518a
URL: http://dx.doi.org/10.1080/10286202100002518a

Molecular Simulation, 2003 Vol. 29 (2), pp. 101–109

Taylor & Francis
Taylor & Francis Group

Molecular-level Calculation Scheme for Pressure in Inhomogeneous Systems of Flat and Spherical Layers

TAMIO IKESHOJI[a,*], BJØRN HAFSKJOLD[a,b] and HILDE FURUHOLT[b]

[a]*Research Institute for Computational Sciences, National Institute of Advanced Industrial Science and Technology, AIST Tsukuba Central 2, Umezono 1-1-1, Tsukuba 305-8568, Japan;* [b]*Department of Chemistry, Norwegian University of Science and Technology, N-7491 Trondheim, Norway*

(Received June 2002; In final form July 2002)

Expressions for the microscopic pressure tensor, suitable for use in molecular dynamics (MD) and Monte Carlo simulations, are presented. The expressions apply to heterogeneous systems consisting of particles interacting with pair-wise additive potentials. The normal and transverse components of the pressure tensor as defined by Irving and Kirkwood [Irving, A.J.H. and Kirkwood, J.G. *J. Chem. Phys.*, 18 (1950) 817] were used to derive explicit equations for the coarse-grained pressure in planar and spherical symmetries. Molecular dynamics simulation results at/near planar and spherical surfaces confirmed that mechanical balance is attained at equilibrium. Furthermore, it was found that the computed coarse-grained pressure in a local volume was more precise than the pressure on a surface for a given simulation length.

Keywords: Pressure tensor; Molecular dynamics; Interfaces; Droplet

INTRODUCTION

Calculation of the microscopic pressure tensor, **P** (or the stress tensor, $-\mathbf{P}$), by molecular dynamics (MD) or Monte Carlo simulations is not trivial for heterogeneous systems due to the pressure tensor's ambiguous definition [1–5]. The computational techniques involved have been discussed by several authors [4,6–16] with an apparent preference for the method of planes (MOP) by Todd *et al.* [8] and the thermodynamic method by Lovett and Baus [9–14]. The MOP implies the Irving–Kirkwood (IK) gauge, whereas the thermodynamic method has some similarities with the Harasima gauge. For planar geometry, the thermodynamic method gives the same local pressure as the transverse components of the pressure tensor defined by Harasima [2,6,9–14,16] whereas the MOP gives the normal component of both the IK and the Harasima pressure tensors [1,6,8,16] (the two definitions lead to identical expressions for the normal component for planar geometry).

The MOP gives the pressure at an imaginary surface in the fluid. For spherical surfaces, Thompson *et al.* derived equations for the normal component of the IK pressure tensor and the transverse component of the Harasima pressure tensor, and applied these to liquid droplets [4]. Thompson *et al.* reported configurational (non-ideal) contributions to the pressure on a surface, whereas the kinetic (ideal) contribution relates to a local volume. One may expect that the coarse-grained pressure, i.e. integrated over a local volume, gives better statistics and thus is more effective, but this is not obvious for the following reason: consider a layer of thickness Δx and assume that this thickness is small compared to size of the particles. The particle pairs contributing to the pressure in Δx will also contribute to the pressure on a plane located in Δx, except for a few pairs with both particles on the same side of the plane. A method to calculate the pressure tensor in a small volume was recently given by Cormier *et al.* [19] for solids, but it is applicable only to systems with a short range potential.

The purpose of the present paper is, therefore, to derive expressions for the corase-grained pressure tensor in a local volume and to examine their statistical efficiency in MD simulations. Our interest in this topic is due to the fact that **P** is needed for several purposes, such as computation of the surface

*Corresponding author.

ISSN 0892-7022 print/ISSN 1029-0435 online
DOI: 10.1080/10286202100002518

tension, Tolman length, and the local heat flux across or along an interface. Although the results will also apply to solid states, the numerical results presented in this paper are valid only for the diagonal elements of **P**.

In a uniform bulk fluid, the α- and β-components of the pressure tensor, $p_{\alpha\beta}$, are:

$$p_{\alpha\beta} = p\delta_{\alpha\beta}, \tag{1}$$

where p is the isotropic pressure and $\delta_{\alpha\beta}$ is Kronecker's delta. The isotropic pressure of N particles in a system volume V_{sys} interacting with a pair-wise additive potential and with no external force may be computed from the virial theorem,

$$p = -\frac{1}{6V_{\text{sys}}}\left\langle \sum_{i=1}^{N}\sum_{\substack{j=1\\ j\neq i}}^{N} \mathbf{r}_{ij}\cdot\mathbf{f}_{ij}\right\rangle + k_{\text{B}}T_{\text{sys}}\rho_{\text{sys}}, \tag{2}$$

where $\mathbf{r}_{ij} = \mathbf{r}_j - \mathbf{r}_i$ is the vector from position $\mathbf{r}_i$ of particle i to $\mathbf{r}_j$, $\mathbf{f}_{ij}$ is the force acting on i due to j, k_{B} is Boltzmann's constant, T_{sys} the temperature, and $\rho_{\text{sys}} = N/V_{\text{sys}}$ the number density. The brackets $\langle\cdots\rangle$ represent an ensemble average. An intuitive modification of Eq. (2) for the pressure tensor in a local volume, V, is to sum up the virial contributions from those pairs with at least one of the particles in V:

$$p_{\alpha\beta}(V) = -\frac{1}{2V}\left\langle \sum_{i\in V}\sum_{j\neq i}(\mathbf{e}_\alpha\cdot\mathbf{r}_{ij})(\mathbf{e}_\beta\cdot\mathbf{f}_{ij})\right\rangle + k_{\text{B}}T(V)\rho(V)\delta_{\alpha\beta} \tag{3}$$

where $T(V)$ and $\rho(V)$ are the local density and temperature in V, respectively, and $\mathbf{e}_\alpha$ and $\mathbf{e}_\beta$ are unit vectors in the α- and β-directions. Equation (3) which is a coarse-grained Irving–Kirkwood-1 (cgIK1) approximation, does not give the correct value of the microscopic pressure tensor when the system is not uniform [8]; it violates the condition of mechanical equilibrium, $\nabla\cdot\mathbf{P} = 0$ [15,16]. This defect of the IK1 approximation was corrected in the MOP, valid for planar surfaces. However, Eq. (3) does give the correct surface tension for an infinite and flat interface, since the errors cancel in the integrated difference between the normal and the transverse pressure components [15,18].

The basic equations for planar and spherical symmetries are given in second section, including a summary of the equations for the pressure at a surface and some new results for the coarse-grained pressure in a local volume. The MD simulations are described in third section, and results for the planar interface and a liquid droplet are discussed in fourth section. Conclusions are given in fifth section. A simple consideration that leads to the same coarse-grained expression as that discussed in the section on "The Coarse-grained Pressure Tensor in a Local Volume" is given in Appendix A. The result is equivalent to Eq. (17) with the Irving-Kirkwood contour.

THE MICROSCOPIC PRESSURE TENSOR

Basic Equations

Expressions for the microscopic pressure tensor were first given by Irving and Kirkwood [1]. The basic principle behind their derivation is the conservation of momentum. This gives an ambiguous definition of the pressure since only the divergence of the pressure and not the pressure itself is defined this way. The microscopic pressure tensor was reformulated by Schofield and Henderson [3], who showed that the ambiguity amounts to an arbitrary choice of an integration contour. Schofield and Henderson considered the components of the local pressure tensor,

$$p_{\alpha\beta}(\mathbf{R}) = \langle p_{c,\alpha\beta}(\mathbf{R})\rangle + \langle p_{k,\alpha\beta}(\mathbf{R})\rangle, \tag{4}$$

where $\mathbf{R}$ is some point in space,

$$p_{c,\alpha\beta}(\mathbf{R}) = \frac{1}{2}\sum_i\sum_{j\neq i} p_{ij,\alpha\beta}(\mathbf{R}) \tag{5}$$

is the configurational contribution to the pressure, and

$$p_{k,\alpha\beta}(\mathbf{R}) = \sum_i m_i[\mathbf{e}_\alpha\cdot(\mathbf{v}_i - \mathbf{u})] \times [\mathbf{e}_\beta\cdot(\mathbf{v}_i - \mathbf{u})]\delta(\mathbf{R} - \mathbf{r}_i) \tag{6}$$

is the kinetic contribution. The pair-wise contribution to the pressure in Eq. (5) is [3]

$$p_{ij,\alpha\beta}(\mathbf{R}) = -\int_{C_{ij}} f_{ij,\alpha}\delta(\mathbf{R} - \mathbf{l})\,\mathrm{d}l_\beta, \tag{7}$$

where $f_{ij,\alpha} = \mathbf{e}_\alpha\cdot\mathbf{f}_{ij}$ is the α-component of $\mathbf{f}_{ij}$, $\delta(\mathbf{R} - \mathbf{l})$ is the Dirac delta function, $\mathbf{l}$ is a position on the integration contour C_{ij} from $\mathbf{r}_i$ to $\mathbf{r}_j$, and $\mathrm{d}l_\beta = \mathbf{e}_\beta\cdot\mathrm{d}\mathbf{l}$. We assume that $\mathbf{f}_{ij}$ and $\mathbf{r}_{ij}$ are parallel, i.e. $\mathbf{f}_{ij} = -f_{ij}\mathbf{r}_{ij}/r_{ij}$ where the derivative of the pair potential is $f_{ij} = -\partial\phi_{ij}/\partial r$. Since $f_{ij,\alpha}$ in general depends on C_{ij}, it is part of the integrand in Eq. (7). In the kinetic contribution, $\mathbf{v}_i$ and m_i are the velocity and mass of particle i, respectively, and $\mathbf{u}$ is the streaming velocity. In this work, we shall consider equilibrium systems for which the kinetic part is

$$\langle p_{k,\alpha\beta}(\mathbf{R})\rangle = k_{\text{B}}T(\mathbf{R})\rho(\mathbf{R})\delta_{\alpha\beta} \tag{8}$$

but Eq. (6) is valid also in non-equilibrium states and when there is a streaming velocity $\mathbf{u}$.

Several authors have discussed the arbitrariness in the choice of C_{ij}[1–3,5,7–14]. Since the purpose of this paper is to examine the efficiency of the computational methods rather than to contribute to

this discussion, we have employed the most popular choice, the IK contour. The IK contour is defined as the straight line between i and j.

The Pressure Tensor at a surface

The pressure at a surface is obtained by solving Eq. (7) for a given choice of C_{ij}. For a planar surface with area A located at $x =$ constant and with the IK contour, the configurational contribution to the pressure is [6,8,16]:

$$p_{ij,\alpha\alpha}(x) = \frac{1}{A}\frac{(r_{ij}^{\alpha})^2}{r_{ij}|x_{ij}|} f_{ij}\,\Theta\left(\frac{x - x_i}{x_j - x_i}\right)\Theta\left(\frac{x_j - x}{x_j - x_i}\right), \qquad (9)$$

where $\alpha = x$, y, or z. The product

$$\Theta\left(\frac{x - x_i}{x_j - x_i}\right)\Theta\left(\frac{x_j - x}{x_j - x_i}\right)$$

equals 1 if x is between x_i and x_j, otherwise it is 0. Equation (9) with $\alpha = x$ is the configurational contribution used in the MOP [8,16].

For a spherical surface located at $R =$ constant in spherical coordinates, the pressure tensor at equilibrium is given by

$$\mathbf{P}(R) = p_{\mathrm{N}}(R)[\mathbf{e}_R\mathbf{e}_R] + p_{\mathrm{T}}(R)[\mathbf{e}_\theta\mathbf{e}_\theta + \mathbf{e}_\phi\mathbf{e}_\phi]. \qquad (10)$$

The normal (radial) and transverse (angular) components for the pair i, j are given by [17]

$$p_{ij,\mathrm{N}}(R) = \frac{m(R)}{4\pi R^3} f_{ij}\, c_{ij} \qquad (11)$$

and

$$p_{ij,\mathrm{T}}(R) = \frac{m(R)}{8\pi R^3} f_{ij}\, c_{ij}\left[\left(\frac{R}{c_{ij}}\right)^2 - 1\right] \qquad (12)$$

with the IK contour. Here, c_{ij} is half the length of the chord given by the intersection between the surface of a sphere of radius R and the line $\mathbf{r}_i + \lambda\mathbf{r}_{ij}$ ($-\infty < \lambda < \infty$) and $m(R)$ is the number of such intersections in $0 \le \lambda \le 1$ ($m(R) = 0, 1, 2$). We shall call the method based on Eqs. (9), (11), and (12) the IK method.

The Coarse-grained Pressure Tensor in a Local Volume

The coarse-grained value of $p_{\alpha\beta}(\mathbf{R})$ is obtained by integrating Eq. (4) over a local volume V (coarse-grained quantities are expressed with "^")

$$\hat{p}_{\alpha\beta} = \frac{1}{V}\int_V p_{\alpha\beta}(\mathbf{R})\,\mathrm{d}R = \langle \hat{p}_{\mathrm{c},\alpha\beta}\rangle + \langle \hat{p}_{\mathrm{k},\alpha\beta}\rangle, \qquad (13)$$

where the non-ideal (configurational) contribution is

$$\hat{p}_{c,\alpha\beta} = \frac{1}{2}\sum_i \sum_{j\neq i} \hat{p}_{ij,\alpha\beta} \qquad (14)$$

with $\hat{p}_{ij,\alpha\beta}$ given by

$$\hat{p}_{ij,\alpha\beta} = -\frac{1}{V}\int_V \left[\int_{C_{ij}} f_{ij,\alpha}\,\delta(\mathbf{R} - 1)\,\mathrm{d}l_\beta\right]\mathrm{d}\mathbf{R}. \qquad (15)$$

The ideal (kinetic) contribution in Eq. (13) is

$$\hat{p}_{k,\alpha\beta} = \frac{1}{V}\sum_{i\in V} m_i[\mathbf{e}_\alpha\cdot(\mathbf{v}_i - u)][\mathbf{e}_\beta\cdot(\mathbf{v}_i - \mathbf{u})] \qquad (16)$$

with summation over all particles in V. Equation (15) may be simplified by exchanging the order of integration:

$$\begin{aligned}\hat{p}_{ij,\alpha\beta} &= -\frac{1}{V}\int_{C_{ij}} f_{ij,\alpha}\left[\int_V \delta(\mathbf{R} - \mathbf{l})\,\mathrm{d}\mathbf{R}\right]\mathrm{d}l_\beta \\ &= -\frac{1}{V}\int_{C_{ij}\in V} f_{ij,\alpha}\,\mathrm{d}l_\beta, \end{aligned} \qquad (17)$$

where $C_{ij} \in V$ means that the pair i, j contributes to the pressure only with the part of C_{ij} that is inside V. Even if neither i nor j is in V, the pair contributes to the pressure tensor if the connecting line passes through V and the interparticle distance is within the range of the pair potential.

The Coarse-grained Pressure Tensor in a Flat Layer in Cartesian Coordinates

As a local volume we consider a flat layer with area A and thickness Δx such that the layer is perpendicular to the x-axis and with $V = A\Delta x$. The system is supposed to be uniform in y- and z-directions. For the IK contour, we define the entry point to be $\mathbf{a} = \{x_a, y_a, z_a\}$ and the exit point to be $\mathbf{b} = \{x_b, y_b, z_b\}$. If i is inside V, then we set $\mathbf{a} = \mathbf{r}_i$. If j is inside V, then we set $\mathbf{b} = \mathbf{r}_j$. For the IK contour, the different situations are indicated by arrows in Fig. 1 for various cases of i and j. The corresponding $\hat{p}_{ij,\alpha\alpha}$ follows from Eq. (17)

$$\hat{p}_{ij,\alpha\alpha} = -\frac{f_{ij,\alpha}}{V}\int_{\alpha_a}^{\alpha_b}\mathrm{d}\alpha = -\frac{f_{ij,\alpha}}{V}\frac{r_{ij,\alpha}}{r_{ij,x}}(x_b - x_a), \qquad (18)$$

where $r_{ij,\alpha} = \mathbf{e}_\alpha\cdot\mathbf{r}_{ij}$. Equation (18) represents the fraction of the virial $\mathbf{r}_{ij}\cdot\mathbf{f}_{ij}$ assigned to each layer according to how much of the contour penetrates the layer. We shall call the method using Eq. (18) the coarse-grained IK (cgIK) method.

In the case that the two particles are in the same layer, Eq. (18) reduces to the ordinary virial expression,

$$\hat{p}_{ij,\alpha\alpha} = -\frac{r_{ij,\alpha} f_{ij,\alpha}}{V}, \quad \alpha = x, y, z. \qquad (19)$$

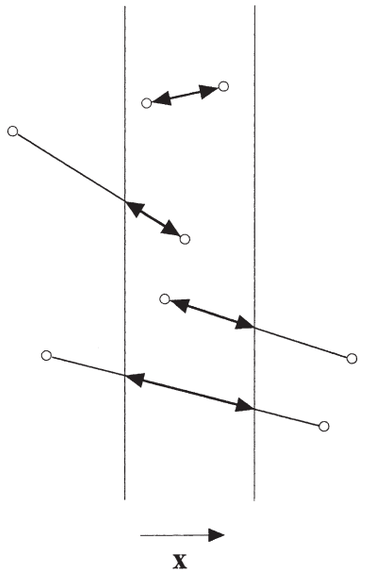

FIGURE 1 Illustration of various particle configurations that contribute to the pressure in a flat layer in Cartesian coordinates. Integration regions are shown by arrows.

The Coarse-grained Pressure Tensor in a Spherical Layer in Spherical Coordinates

Here we consider a droplet at the center of a spherical coordinate system and a local volume in the form of a spherical shell of radius R and thickness ΔR.

For the IK choice of C_{ij}, the possible situations that contribute to the pressure in V are shown in Fig. 2. A point $\mathbf{l}(\lambda)$ on the contour is specified by the scalar λ:

$$\mathbf{l}(\lambda) = \mathbf{r}_i + \lambda \mathbf{r}_{ij}; \quad 0 \le \lambda \le 1. \tag{20}$$

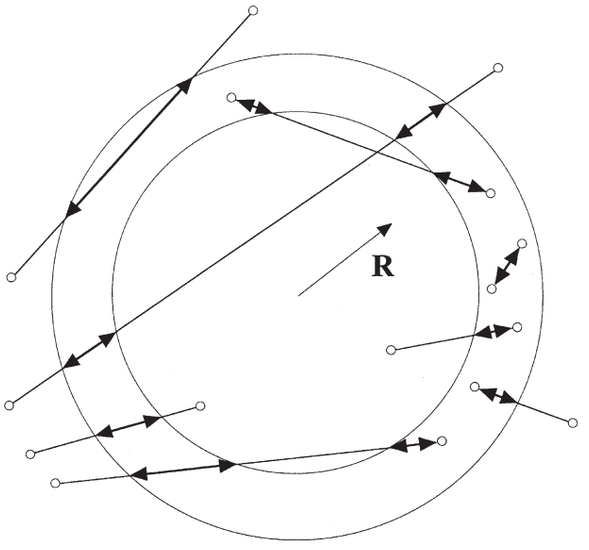

FIGURE 2 Illustration of various particle configurations that contribute to the pressure in a spherical layer in spherical coordinates. Integration regions are shown by arrows.

We will also need $l = |\mathbf{l}|$, which is a function of λ. The interval $C_{ij} \in V$ is defined by $\lambda_a \le \lambda \le \lambda_b$ where λ_a and λ_b are given by $\mathbf{a} = \mathbf{r}_i + \lambda_a \mathbf{r}_{ij}$ and $\mathbf{b} = \mathbf{r}_i + \lambda_b \mathbf{r}_{ij}$, respectively, and $\mathbf{a}$ and $\mathbf{b}$ are the entry and exit points, respectively, of C_{ij} in V. For some configurations of i and j, C_{ij} may penetrate V twice as seen in Fig. 2, and $C_{ij} \in V$ represents two separate intervals. These situations will be understood in the following as the integral $\int_{\lambda_a}^{\lambda_b}$ actually consisting of two parts ($\int_{\lambda_a}^{\lambda_b} + \int_{\lambda_{a'}}^{\lambda_{b'}}$), without being explicitly shown. Furthermore, we assume the notation that $\lambda_a = 0$ if $\mathbf{r}_i \in V$ and $\lambda_b = 1$ if $\mathbf{r}_j \in V$. The value of λ at the surface of the sphere of radius R is

$$\lambda_R = \lambda_0 \pm \frac{1}{r_{ij}} \sqrt{R^2 - l_0^2} \tag{21}$$

with $0 < \lambda_R < 1$. The closest distance from origin to $\mathbf{l}(\lambda)$ is

$$l_0 = \sqrt{r_i^2 - \left(\frac{\mathbf{r}_i \cdot \mathbf{r}_{ij}}{r_{ij}}\right)^2}, \tag{22}$$

and λ_0 is the corresponding value: $l_0 = |\mathbf{r}_i + \mathbf{r}_{ij}\lambda_0|$.

The $\hat{p}_{ij,\alpha\beta}$ in V follows from Eq. (17)

$$\hat{p}_{ij,\alpha\beta} = -\frac{1}{V} \int_{\lambda_a}^{\lambda_b} (\mathbf{e}_\alpha \cdot \mathbf{f}_{ij})(\mathbf{e}_\beta \cdot \mathbf{r}_{ij})\, \mathrm{d}\lambda. \tag{23}$$

Note that the unit vectors $\mathbf{e}_r$, $\mathbf{e}_\theta$, and $\mathbf{e}_\phi$ are not constant along the contour $\mathbf{l}(\lambda)$; expressed in Cartesian coordinates they are

$$\begin{aligned}
\mathbf{e}_r &= \left\{ \frac{l_x}{l}, \frac{l_y}{l}, \frac{l_z}{l} \right\} \\
\mathbf{e}_\theta &= \left\{ \frac{l_x l_z}{l(l_x^2 + l_y^2)^{1/2}}, \frac{l_y l_z}{l(l_x^2 + l_y^2)^{1/2}}, -\frac{(l_x^2 + l_y^2)^{1/2}}{l} \right\} \\
\mathbf{e}_\phi &= \left\{ -\frac{l_y}{(l_x^2 + l_y^2)^{1/2}}, \frac{l_x}{(l_x^2 + l_y^2)^{1/2}}, 0 \right\}
\end{aligned} \tag{24}$$

where θ is the angle between the z-axis and $\mathbf{l}$, ϕ is the azimuth angle in the x-, y-plane, and l_α is the α-component of $\mathbf{l}$. The angle θ may also be defined relative to the x- or y-axis. By symmetry, all three definitions must give identical results for the transverse pressure component. Using the unit vectors given by Eq. (24), the normal and transverse pressure components may now be written as

$$\hat{p}_{ij,\mathrm{N}} = \frac{f_{ij}}{r_{ij} V} \int_{\lambda_a}^{\lambda_b} \left[\frac{r_{ij}^4 \lambda^2 + 2(\mathbf{r}_i \cdot \mathbf{r}_{ij}) r_{ij}^2 \lambda + (\mathbf{r}_i \cdot r_{ij})^2}{r_{ij}^2 \lambda^2 + 2(\mathbf{r}_i \cdot \mathbf{r}_{ij})\lambda + r_i^2} \right] \mathrm{d}\lambda \tag{25}$$

$$\hat{p}_{ij,\phi\phi} = \frac{f_{ij}}{r_{ij}V}(r_{i,y}r_{ij,x} - r_{i,x}r_{ij,y})^2 \times \int_{\lambda_a}^{\lambda_b} \left[\frac{1}{r_{ij,xy}^2\lambda^2 + 2(\mathbf{r}_{i,xy}\cdot\mathbf{r}_{ij,xy})\lambda + r_{i,xy}^2} \right] \mathrm{d}\lambda, \quad (26)$$

where $\mathbf{r}_{i,xy}$ and $\mathbf{r}_{ij,xy}$ are the projections of $\mathbf{r}_i$ and $\mathbf{r}_{ij}$, respectively, onto the x, y-plane. The integrands have the following geometrical interpretations:

The denominator of the integrand in Eq. (25) is the square of $\mathbf{l}$, l^2, given as

$$l(\lambda)^2 = r_{ij}^2\lambda^2 + 2(\mathbf{r}_i\cdot\mathbf{r}_{ij})\lambda + r_i^2. \quad (27)$$

The numerator is $r_{ij}^4(\lambda - \lambda_0)^2 = r_{ij}^2[l(\lambda)^2 - l_0^2]$ where $[l(\lambda)^2 - l_0^2]$ is the square of the chord length between $\mathbf{l}(\lambda)$ and $\mathbf{l}(\lambda_0)$. The denominator of the integrand in Eq. (26) is the square of the projection of $\mathbf{l}$ onto the x, y-plane, l_{xy}^2. The minimum value of l_{xy} is

$$l_{xy,0} = \sqrt{r_{i,xy}^2 - \left(\frac{\mathbf{r}_{i,xy}\cdot\mathbf{r}_{ij,xy}}{r_{ij,xy}} \right)^2} \quad (28)$$

(the closest distance from origin to the straight line through $\mathbf{r}_{i,xy}$ and $\mathbf{r}_{j,xy}$) and the corresponding value of λ is $\lambda_{xy,0}$. In general, $\lambda_{xy,0} \neq \lambda_0$. The factor $(r_{i,y}r_{ij,x} - r_{i,y}r_{ij,x} - r_{i,x}r_{ij,y})$ is the projection of $\mathbf{r}_{ij,xy}$ onto the ϕ-direction unit vector at position $\mathbf{r}_{i,xy}$ $(\mathbf{e}_{i,\phi})$, multiplied with r_i, i.e.

$$r_{i,y}r_{ij,x} - r_{i,x}r_{ij,y} = r_i(\mathbf{e}_{i,\phi}\cdot r_{ij,xy}). \quad (29)$$

The integrals may be expressed in closed form as

$$\hat{p}_{ij,\mathrm{N}} = \frac{f_{ij}}{V}[r_{ij}(\lambda_b - \lambda_a) + F(\lambda_b) - F(\lambda_a)], \quad (30)$$

where

$$F(\lambda) = -l_0 \arctan\left(\frac{\sqrt{l(\lambda)^2 - l_0^2}}{l_0} \right) \quad (31)$$

and

$$\hat{p}_{ij,\phi\phi} = \frac{f_{ij}}{r_{ij}V}[G(\lambda_b) - G(\lambda_a)], \quad (32)$$

where

$$G(\lambda) = -\frac{(r_{i,y}r_{ij,x} - r_{i,x}r_{ij,y})^2}{r_{ij,xy}l_{xy,0}} \arctan\left(\frac{\sqrt{l_{xy}(\lambda)^2 - l_{xy,0}^2}}{l_{xy,0}} \right). \quad (33)$$

If $l_0 = 0$, i.e. particles i and j are on the same line from the center, then

$$\hat{p}_{ij,\mathrm{N}} = \frac{f_{ij}r_{ij}}{V}(\lambda_b - \lambda_a). \quad (34)$$

If $l_{xy,0} = 0$, i.e. projections of particles i and j onto the x, y plane are on the same line from the center, then

$$\hat{p}_{ij,\phi\phi} = 0. \quad (35)$$

The computational method based on Eqs. (30) and (32) will also be called the cgIK method here, the actual geometry will distinguish it from the cgIK method introduced in "The Coarse-grained Pressure Tensor in a Flat Layer in Cartesian Coordinates" Section.

The transverse pressure component may alternatively be derived in terms of the angle ω of rotation from $\mathbf{r}_i$ to $\mathbf{r}_j$ in the plane defined by these two vectors. The resulting expression for $\hat{p}_{ij,\omega\omega}$ is

$$\hat{p}_{ij,\omega\omega} = -\frac{f_{ij}}{V}[F(\lambda_b) - F(\lambda_a)]. \quad (36)$$

Although the pairwise contributions $\hat{p}_{ij,\phi\phi}$ [Eq. (32)] and $\hat{p}_{ij,\omega\omega}$ [Eq. (36)] are different, they give the same ensemble average of the configurational part (apart from a factor 1/2 due to the fact that the rotation ω incorporates both rotations ϕ and θ),

$$\left\langle \frac{1}{2}\sum_i\sum_{j\neq i}\hat{p}_{ij,\phi\phi} \right\rangle = \left\langle \frac{1}{4}\sum_i\sum_{j\neq i}\hat{p}_{ij,\omega\omega} \right\rangle = \hat{p}_{\mathrm{c,T}}(R). \quad (37)$$

MD SIMULATIONS

Molecular dynamics simulations were carried out for a one-component system using the Lennard-Jones potential $\phi(r)$ with a switching function centered at $r_s^* \equiv r_s/\sigma = 2.5$ [20]:

$$\phi(r) = 4\varepsilon\left[\left(\frac{\sigma}{r}\right)^{12} - \left(\frac{\sigma}{r}\right)^{6} \right] S(r), \quad (38)$$

where

$$S(r) = \left[1 + \frac{r}{r_s} \right]^{-24}. \quad (39)$$

In the planar case, a tetragonal unit cell with aspect ratios $L_x/L_y = L_x/L_z = 2$ was divided into layers of equal thickness $\Delta x^* \equiv \Delta x/\sigma = 0.2$ or 0.4 and perpendicular to the x-axis as shown in Fig. 3a (variables marked with an asterisk are in reduced Lennard-Jones units). Details are presented elsewhere [21]. In the case of the droplet, a cubic unit cell was divided into spherical layers of equal thickness $\Delta R^* = 0.2$ and centered at the center of the cell as shown in Fig. 3b. In both cases, periodic boundary conditions were applied in all directions. Initial 5×10^5–10^6 time steps were made with local thermostatting at different temperatures to establish a liquid/vapor two-phase system, a liquid sheet for planar geometry and a liquid drop for spherical

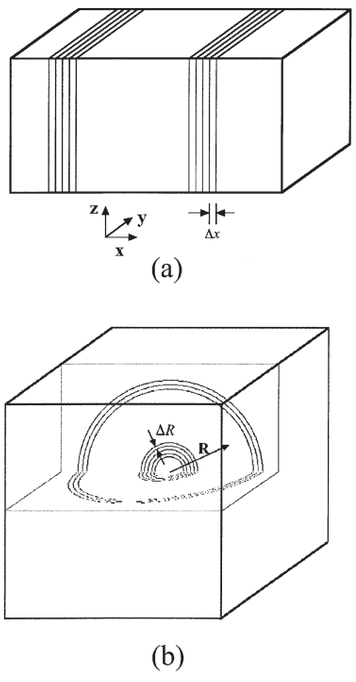

FIGURE 3 Unit cells used for pressure tensor calculation with (a) flat layers and (b) spherical layers.

geometry. Then, *NVE* MD calculations were performed for the two-phase system at $T^* \approx 0.86$ with the parameters given in Table I.

The overall density of the system was chosen so that the gas and liquid volumes were about equal in the planar case, and so that the drop diameter was about 2/3 of the unit cell length in the spherical case. The center of mass of the system was moved to the center of the unit cell at fixed intervals to avoid a drift that would destroy calculation of the average local variables. The simulations were carried out at equilibrium with zero streaming velocity.

The coarse-grained configurational pressure tensor in V was computed from Eq. (18) for planar geometry and Eqs. (30) and (32) for spherical geometry. For both geometries, the kinetic contribution was computed from Eq. (16). The expressions were evaluated every 20th time step for runs 1 and 2, and every 100th time step for runs 3 and 4.

The MOP was used for the x-components in planar geometry according to Eq. (6) evaluated every time step for the kinetic contribution and Eq. (9) evaluated every 20th time step for the configurational contribution.

TABLE I Parameters used in the simulations

Run No.	*1*	*2*	*3*	*4*
N	4096	4096	6080	32768
Geometry	Planar	Planar	Planar	Spherical
δt^*	0.002	0.002	0.005	0.005
Length of run (time steps)	2×10^6	2×10^6	10^7	10^7
Δx^* or ΔR^*	0.2	0.4	0.2	0.2

RESULTS AND DISCUSSION

Pressure Tensor Through a Flat Interface

The normal and transverse components of **P** from the cgIK and cgIK1 methods (Run 3, planar geometry) are shown as function of x^* in Fig. 4 together with the density profile. The temperature is constant ($T^* \approx 0.86$) through the system. The normal component of the cgIK pressure tensor is completely constant through the interface, showing that mechanical equilibrium is attained as required. The transverse components have a dip because of the tension of the interface. The pressure profile using the cgIK1 method has the well-known wavy normal component at/near the interface, which represents a violation of mechanical equilibrium. Although this wave is an artifact of the method, the method does give the correct surface tension, and may for that reason be preferred due to its lower computational effort [15]. This wave does not occur when the pressure is calculated on planes in the system [6,8]. The transverse components obtained from Eqs. (3) and (18) agree well, but not perfectly. We have no way to judge which of these profiles is preferable.

The cgIK1 method samples the pressure in a given layer only when there is a particle in that layer, whereas the IK method, its coarse-grained version cgIK, and the MOP all sample the pressure when the force between two interacting particles penetrate that layer. One should therefore expect that the precision of the cgIK1 method is less than for the other methods. This difference between the cgIK1 method and the other methods must be more pronounced for the normal than for the transverse pressure

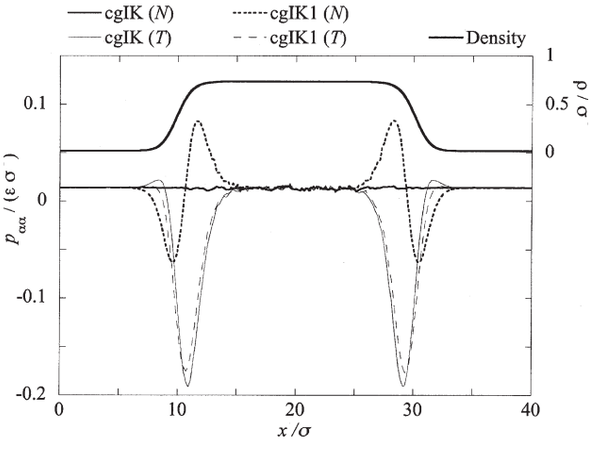

FIGURE 4 Normal (N) and transverse (T) pressure tensor components obtained with the cgIK and cgIK1 methods for planar geometry (Run 3). The upper curve is the density profile.

TABLE II Standard error in the average pressure (in reduced Lennard-Jones units)

	Run 1		*Run 2*	
	Gas	*Liquid*	*Gas*	*Liquid*
cgIK (N)	0.00017	0.00092	0.00017	0.00075
MOP (N)	0.00017	0.00105	0.00017	0.00107
cgIK1 (N)	0.00015	0.00204	0.00014	0.00125
cgIK (T)	0.00023	0.00198	0.00021	0.00163
cgIK1 (T)	0.00021	0.00199	0.00020	0.00161

components, and especially in the liquid phase, where the kinetic and configurational contributions are both large and of opposite sign. A summary of the standard errors in the average pressure components is given in Table II.

The cgIK and MOP give about the same standard error for the normal pressure component in the gas phase, and the cgIK is slightly better in the liquid phase, especially for the thicker layers (Run 2). The cgIK1 also shows the same error in the gas phase, but is significantly less precise in the liquid. The transverse pressure components from the cgIK and cgIK1 methods give the same accuracy, again about an order of magnitude less precise in the liquid compared with the gas.

The small, but significant difference between the cgIK method and the MOP is shown in Fig. 5a and 5b for runs 1 and 2, respectively. For a layer thickness $\Delta x^* = 0.2$ there is little difference between the two methods, but for $\Delta x^* = 0.4$ the difference is noticeable. As Δx^* becomes smaller, the two methods become equivalent. A larger layer thickness than $\Delta x^* = 0.4$ would not be suitable because the datapoints would be too far apart to show the details of the interface. This would be even more pronounced at lower temperatures because of the thinner interface.

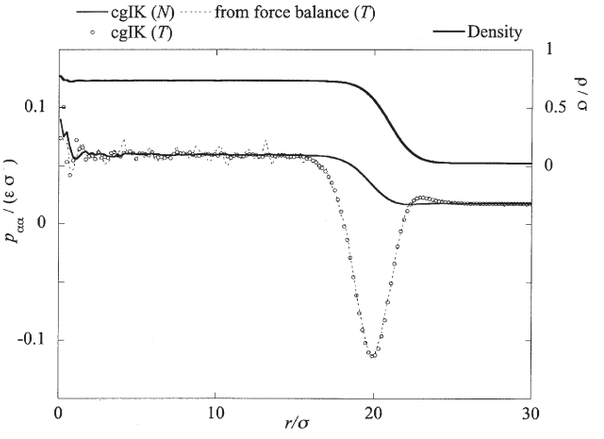

FIGURE 6 Normal (N) and transverse (T) pressure tensor components obtained with the cgIK method for spherical geometry (Run 4). The upper curve is the density profile. The transverse component from the mechanical balance Eq. (40) is also shown.

Pressure Tensor Through a Spherical Interface

The transverse component of the pressure tensor was obtained from the three projections discussed in "The Coarse-grained Pressure Tensor in a Spherical Layer in Spherical Coordinates" Section. The three estimates agreed within statistical error as they should do in the present case of a spherical droplet, and the average is shown in Fig. 6 marked "cgIK (T)". The condition of mechanical equilibrium in spherical coordinates reads

$$p_T(R) = p_N(R) + \frac{2}{R}\frac{dp_N(R)}{dR} \tag{40}$$

or

$$p_N(R) = \frac{2}{R^2}\int_0^R p_T(R)dR. \tag{41}$$

This condition was checked from the independent calculations of $\hat{p}_T$ and $\hat{p}_N$. The $\hat{p}_T$ computed from

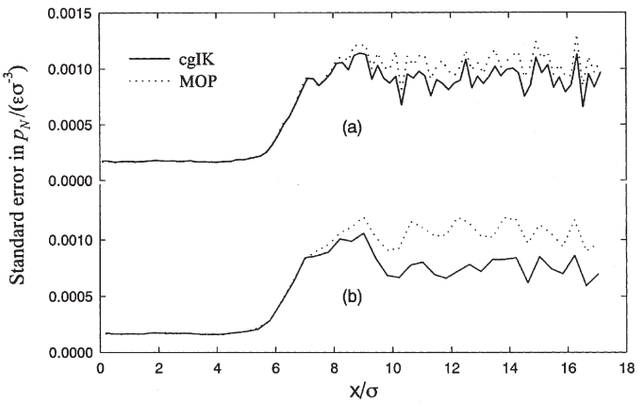

FIGURE 5 Comparison of the precisions of the cgIK method and the MOP. Layer thicknesses are (a) $\Delta x^* = 0.2$ (Run 1) and (b) $\Delta x^* = 0.4$ (Run 2).

Eq. (40) is compared with the results computed from Eq. (32) (and Eq. (16)) in Fig. 6. We find that the two routes to $\hat{p}_T$ agree perfectly.

Thompson *et al.* [4] computed the normal IK pressure from

$$p_N(R)^{(\mathrm{IK})} \frac{1}{4\pi R^3} \left\langle \sum_{i-j\,\mathrm{pair}} \frac{|\mathbf{R}\cdot\mathbf{r}_{ij}|}{r_{ij}} f_{ij} \right\rangle + k_B T(V)\rho(V). \quad (42)$$

Results from this method were compared with those from Eq. (30) (and Eq. (16)), and the agreement was found to be good. This is no surprise because Eq. (30) is obtained by an integration of the pressure on planes. A benefit of the present pressure tensor calculation scheme for the droplet is that both the normal and the transverse components can be obtained for the same contour, while Ref. [4] gave only the normal component with the IK-contour (and the transverse component with the H-contour).

CONCLUSION

By integrating the IK expression for the pressure tensor at a point, the coarse-grained pressure tensors in a local volume (planar and spherical layers) were obtained. The non-ideal term represents the fraction of the virial that corresponds to the fraction of the connecting line in each local volume. The calculated pressure tensors in systems with either a flat or a spherical vapor/liquid interface satisfied the mechanical balance as they should do.

The cgIK gave equal or better precision for the normal component of the pressure tensor than the MOP did. The cgIK1 method gave the same precision as the cgIK method and the MOP for the normal pressure component in gas phase, but less precise results in the liquid phase. The transverse pressure components were equally precise for the cgIK and cgIK1 methods. The MOP does not give the transverse component.

Acknowledgements

TI and BH are grateful to NTNU and AIST, respectively, for their hospitality during stays at these institutions.

References

[1] Irving, A.J.H. and Kirkwood, J.G. (1950) "The statistical mechanical theory of transport processes. IV. The equations of hydrodynamics", *J. Chem. Phys.* **18**, 817.
[2] Harasima, A. (1952) "Molecular theory of surface tension", *Adv. Chem. Phys.* **1**, 203.
[3] Schofield, P. and Henderson, J.R. (1982) "Statistical-mechanics of inhomogeneous fluids", *Proc. R. Soc. Lond.* **A379**, 231.
[4] Thompson, S.M., Gubbins, K.E., Walton, J.P.R.B., Chantry, R.A.R. and Rowlinson, J.S. (1984) "A molecular-dynamics study of liquid-drops", *J. Chem. Phys.* **81**, 530.
[5] Blokhuis, E.M. and Bedeaux, D. (1992) "Pressure tensor of a spherical interface", *J. Chem. Phys.* **97**, 3576.
[6] Walton, J.P.R.B., Tildesley, D.J. and Rowlinson, J.S. (1983) "The pressure tensor at the planar surface of a liquid", *Mol. Phys.* **48**, 1357.
[7] Rowlinson, J.S. (1994) "A drop of liquid", *J. Phys. Condens. Mat.* **6**, A1.
[8] Todd, B.D., Evans, D.J. and Daivis, P.J. (1995) "Pressure tensor for inhomogeneous fluids", *Phys. Rev. E* **52**, 1627.
[9] Lovett, R. and Baus, M. (1991) "A family of equivalent expressions for the pressure of a fluid adjacent to a wall", *J. Chem. Phys.* **95**, 1991.
[10] Lovett, R. and Baus, M. (1992) "Molecular scale force distributions associated with a planar interface", *J. Chem. Phys.* **97**, 8596.
[11] Baus, M. and Lovett, R. (1995) "The magnitude and location of the surface-tension of curved interfaces", *J. Chem. Phys.* **103**, 377.
[12] Lovett, R. and Baus, M. (1997) "A molecular theory of the Laplace relation and of the local forces in a curved interface", *J. Chem. Phys.* **106**, 635.
[13] Mareschal, M., Baus, M. and Lovett, R. (1997) "The local pressure in a cylindrical liquid–vapor interface: a simulation study", *J. Chem. Phys.* **106**, 645.
[14] El Bardouni, H., Mareschal, M. and Lovett, R. (2000) "Computer simulation study of the local pressure in a spherical liquid–vapor interface", *J. Chem. Phys.* **113**, 9804.
[15] Nijmeijer, M.L.P., Bakker, A.F., Bruin, C. and Sikkenk, J.H. (1988) "A molecular dynamics simulation of the Lennard-Jones liquid–vapor interface", *J. Chem. Phys.* **89**, 3789.
[16] Varnik, F., Baschnagel, J. and Binder, K. (2000) "Molecular dynamics results on the pressure tensor of polymer films", *J. Chem. Phys.* **113**, 4444.
[17] Hafskjold, B. and Ikeshoji, T. (2002) "The microscopic pressure tensor for hard-sphere fluids", *Phys. Rev. E* **66**, 011203.
[18] Chen, Li-Jen (1995) "Area dependence of the surface-tension of a Lennard-Jones fluid from molecular-dynamics simulations", *J. Chem. Phys.* **103**, 10214.
[19] Cormier, J., Rickman, J.M. and Delph, T.J. (2001) "Stress calculation in atomistic simulations of perfect and imperfect solids", *J. Appl. Phys.* **89**, 99.
[20] Ikeshoji, T. and Hafskjold, B. (1994) "Nonequilibrium molecular-dynamics calculation of heat-conduction in liquid and through liquid–gas interface", *Mol. Phys.* **81**, 251.
[21] Hafskjold, B. and Ikeshoji, T. (1996) "Non-equilibrium molecular dynamics simulation of coupled heat- and mass-transport across a liquid vapor interface", *Mol. Simul.* **16**, 139.

APPENDIX A

In order to obtain Eq. (7) for the pressure defined at a point, Irving and Kirkwood used the pressure difference that produces a momentum flow. It is possible to use a more direct and mechanical definition; the pressure is a force per unit surface area. However, the ambiguity discussed in the Introduction still remains, since the local surface where the force acts is not determined without ambiguity, i.e. we do not know where the force acts. The pressure on an infinitely large surface S may be expressed as a sum of ideal and non-ideal terms due to particles traveling through, and forces acting through the plane, respectively. The ideal term will be in the same form as Eq. (6) and the coarse-grained value is easily obtained as Eq. (16). Therefore, we consider only the non-ideal term, $p_{c,S}$, which can be expressed by the sum of force components, $f_{ij,n}$ (normal to the surface), that act between all pairs of particles i and j, located at the left and right sides of

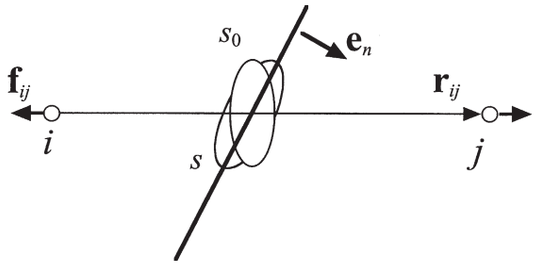

FIGURE 7 Pressure due to i–j pair (see text for explanation of the symbols).

an infinitely large surface, respectively. This gives

$$p_{c,S} = \frac{1}{S} \sum_{i \in \text{left}} \sum_{j \in \text{right}} f_{ij,n}. \tag{43}$$

For a repulsive force, $f_{ij,n}$ is positive. As an extension of this idea, the contribution from an i–j pair to the pressure on a small part of S, through which the i–j connecting line passes, may be defined as

$$p_{ij,n} = \frac{f_{ij,n}}{s} = -\text{sign}\left(\frac{\mathbf{e}_n \cdot \mathbf{f}_{ij}}{s}\right), \tag{44}$$

where s is the area of the small surface and $\mathbf{e}_n$ is the unit vector normal to s. In this equation, the force is assumed to act through the surface s as shown in Fig. 7. This corresponds to the IK choice for the integration contour. By an arbitrary convention, we choose sign to be positive when $\mathbf{e}_n$ points towards particle j and negative when $\mathbf{e}_n$ points towards i. Introducing a surface normal to the i–j connecting line, $s_0 (= \text{sign}\, s(\mathbf{e}_n \cdot \mathbf{r}_{ij})/r_{ij})$, Eq. (44) becomes

$$p_{i,j,n} = -\frac{(\mathbf{e}_n \cdot \mathbf{r}_{ij})(\mathbf{e}_n \cdot \mathbf{f}_{ij})}{r_{ij} s_0}. \tag{45}$$

When the surface s is moved from position a to b, both of which are on the i–j connecting line, it is possible to calculate an average pressure $\bar{p}_{ij,ab}$ between a and b by integrating Eq. (45) as

$$\bar{p}_{ij,ab} = \frac{1}{V_{ab}} \int_a^b p_{ij,n} s_0 \, \mathrm{d}q, \tag{46}$$

where q is the coordinate along the connecting line and

$$V_{ab} = \int_a^b s_0 \, \mathrm{d}q \tag{47}$$

is the volume swept by the surface from a to b. We now make s_0 infinitesimal and choose a and b such that V_{ab} is entirely within the local volume V. The average pressure will then contribute to the total pressure by V_{ab}/V. Thus, the non-ideal part of the pressure due to the i–j pair in the local volume is given by

$$\hat{p}_{ij,n} = \bar{p}_{ij,ab} \frac{V_{ab}}{V}. \tag{48}$$

Introducing Eqs. (45)–(47) into Eq. (48), it becomes

$$\hat{p}_{ij,n} = -\frac{1}{r_{ij} V} \int_a^b [(\mathbf{e}_n \cdot \mathbf{r}_{ij})(\mathbf{e}_n \cdot \mathbf{f}_{ij})] \, \mathrm{d}q. \tag{49}$$

This $\hat{p}_{ij,n}$ is the same as the coarse-grained normal component $\hat{p}_{ij,\alpha\beta}$ (with $\alpha = \beta$ corresponding to the normal component) given by Eq. (17).